Registration-based segmentation with articulated model from multipostural magnetic resonance images for hand bone motion animation

Hsin-Chen Chen[a)]
Department of Computer Science and Information Engineering, National Cheng Kung University, No. 1, University Road, Tainan 701, Taiwan, Republic of China

I-Ming Jou[b)]
Department of Orthopedics, College of Medicine, National Cheng Kung University, No. 138, Sheng Li Road, Tainan 704, Taiwan, Republic of China

Chien-Kuo Wang[c)]
Department of Radiology, National Cheng Kung University Hospital, No. 138, Sheng Li Road, Tainan 704, Taiwan, Republic of China

Fong-Chin Su[d)]
Institute of Biomedical Engineering, National Cheng Kung University, No. 1, University Road, Tainan 701, Taiwan, Republic of China

Yung-Nien Sun[e)]
Department of Computer Science and Information Engineering, National Cheng Kung University, No. 1, University Road, Tainan 701, Taiwan, Republic of China and Department of Computer Science and Information Engineering, National Pingtung Institute of Commerce, No. 51, Min Sheng E. Road, Pingtung 900, Taiwan, Republic of China

(Received 8 October 2009; revised 26 February 2010; accepted for publication 25 March 2010; published 19 May 2010)

Purpose: The quantitative measurements of hand bones, including volume, surface, orientation, and position are essential in investigating hand kinematics. Moreover, within the measurement stage, bone segmentation is the most important step due to its certain influences on measuring accuracy. Since hand bones are small and tubular in shape, magnetic resonance (MR) imaging is prone to artifacts such as nonuniform intensity and fuzzy boundaries. Thus, greater detail is required for improving segmentation accuracy. The authors then propose using a novel registration-based method on an articulated hand model to segment hand bones from multipostural MR images.
Methods: The proposed method consists of the model construction and registration-based segmentation stages. Given a reference postural image, the first stage requires construction of a drivable reference model characterized by hand bone shapes, intensity patterns, and articulated joint mechanism. By applying the reference model to the second stage, the authors initially design a model-based registration pursuant to intensity distribution similarity, MR bone intensity properties, and constraints of model geometry to align the reference model to target bone regions of the given postural image. The authors then refine the resulting surface to improve the superimposition between the registered reference model and target bone boundaries.
Results: For each subject, given a reference postural image, the proposed method can automatically segment all hand bones from all other postural images. Compared to the ground truth from two experts, the resulting surface image had an average margin of error within 1 mm (mm) only. In addition, the proposed method showed good agreement on the overlap of bone segmentations by dice similarity coefficient and also demonstrated better segmentation results than conventional methods.
Conclusions: The proposed registration-based segmentation method can successfully overcome drawbacks caused by inherent artifacts in MR images and obtain more accurate segmentation results automatically. Moreover, realistic hand motion animations can be generated based on the bone segmentation results. The proposed method is found helpful for understanding hand bone geometries in dynamic postures that can be used in simulating 3D hand motion through multipostural MR images.
[DOI: 10.1118/1.3395580]

Key words: MR, hand bones, image segmentation, registration, articulated model

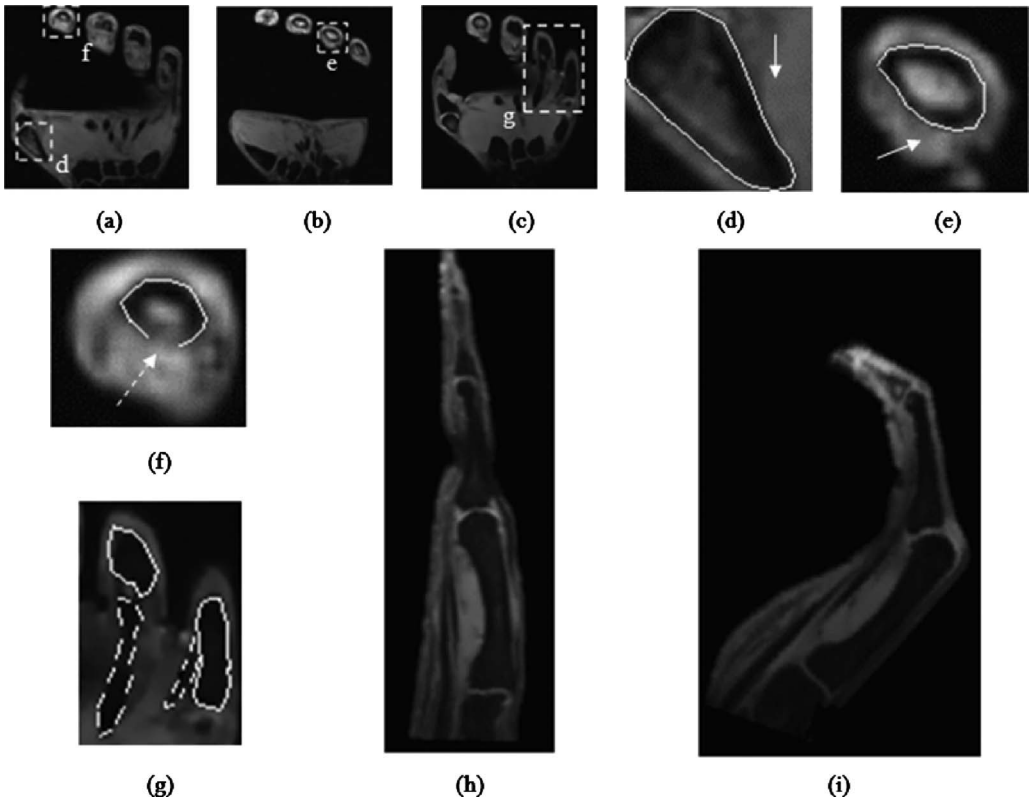

FIG. 1. Four categories of difficulties in automatic segmentation for hand bones. The three slices from (a) to (c) are selected from the hand MR volume images. In order to detail the image, the four windows in (a)–(c) are enlarged in (d)–(g); [(d) and (e)] DY1: Nonuniform intensity distribution inside the hand bones; (f) DY2: Fuzzy bone boundaries; (g) DY3: Confusion by nonrelevant tissue edges; [(h) and (i)] DY4: Large movement between the sampled postures.

I. INTRODUCTION

The human hand is undoubtedly the epitome of a useful and essential tool, invaluable for performing complex tasks with ease and grace. Unfortunately, long-term activities or heavy loads may cause hands to lose dexterity and function, developing symptoms such as "trigger finger."[1] Investigating pathological and biomechanical causes of hand disorders thus makes hand kinematics a vital research field.

Most previous hand kinematics research[2–4] has focused on analyses of hand motion, primarily derived from data attained through skin-surface markers which were tracked by an optical motion capture system. Unfortunately, this methodology potentially decreases the accuracy of tracked maker locations due to skin movement or muscle contraction. Although there has been a rapid development of noninvasive imaging scanners such as magnetic resonance (MR) and computer tomography (CT) that can capture three-dimensional (3D) geometries of internal human structures, these devices mostly provide high quality images for static 3D organs. On the other hand, four-dimensional [(4D), 3D +time] ultrasound devices are able to image the motion of a 3D organ, but they may not be very ideal for studying hand kinematics due to poor spatial resolution and limited field of view. Using images of sequentially moving postures from CT or MR is a better alternative for visualizing high quality 4D motion after interpolating images between adjacent postures. In this study, MR was the selected imaging tool to prevent radiation overexposure in sequential CT imaging.

Recently, there have been several kinematics-related studies and clinical applications based on bone structure segmentation. For instance, Hu *et al.*[5] and Snel *et al.*[6] segmented the bones from MR and CT images and simulated the bone motion of the ankle and wrist, respectively. Miyata *et al.*[7] and Ryu *et al.*[8] also measured the hand kinematic parameters by using the segmented bone information from MR images. On the other hand, the hand joint space, which is an important joint degeneration parameter to diagnose or grade the hand osteoarthritis,[9,10] is measured based on the reconstructed hand bone structures. Furthermore, the hand bone geometries in moving postures help the clinicians to evaluate the functional workspace of the human hand.[11] Unfortunately, the lack of research dedicated to automatic segmentation of hand bones from MR images means that manual segmentation, albeit tedious and time-consuming, is the most common approach for hand bone segmentation. Our research aims to explore and develop a reliable segmentation method of hand bones for moving postural MR images.

The characteristics of MR hand images usually cause difficulties in automatic segmentation, which are roughly classified into four categories as shown in Fig. 1. In ideal fat-suppressed $T2$-weighted MR image acquisition, the bone intensities should be uniform and relatively less than the

muscle intensities, as indicated by the solid arrows. Unfortunately, the fat-suppression techniques usually suffer from susceptibility artifacts of MR imaging,[12] causing bone intensities inside the contours to become heterogeneous. This imperfection is often seen in MR images, e.g., Figs. 1(d) and 1(e), which causes the first kind of difficulty (DY1) in MR image segmentation. Furthermore, due to the partial volume artifact, the intensity gradients of object boundaries may also be nonuniform and cause vague contours or even gaps, as indicated by the dashed arrow in Fig. 1(f). This case makes hand bone segmentation unstable and causes the second type of difficulty (DY2). In Fig. 1(g), the boundaries of bones and tendons are delineated by the solid and dashed contours, respectively. The intensities of bones are quite similar to those of tendons, which cause the third type of difficulty (DY3) in automatically defining the boundaries between them. Since a hand has five fingers with multiple joints and each joint is with a certain degree of freedom (DoF), it has a complicated articulated structure that allows large movements and can generate very different postures, such as the neutral and flexion postures in Figs. 1(h) and 1(i). Therefore, a large movement between two sampled postures cannot be simply described by a rigid or affine transformation. This is the fourth difficulty (DY4) in automatic segmentation.

In the past, deformable model-based segmentation methods[13–15] were commonly used to extract the object contour from images. Two representative approaches, the 2D active contour model [(ACM), snakes)][13] and the active shape model (ASM),[14] achieve segmentation by deforming a contour/surface to capture the strong edges of a target object. Unfortunately, strong edges do not appear consistently throughout the entire contour and strong image noises may exist, producing instability using traditional ACM and ASM. On the other hand, as the initial model in a deformable model-based segmentation is often obtainable by registration, integration of segmentation and registration are complementary and thus compose the registration-based segmentation as exemplified by Zagrodsky *et al.*[16] in a proposal for a deformable model-based framework. They presented a registration-assisted method to segment the cardiac surface from 4D echocardiographic data and then visualize it at different phases of the cardiac cycle. Based on the mutual information-based registration, they resolved the low spatial correlation problems of adjacent image frames caused by heartbeats. Such a registration-based segmentation concept was also utilized in atlas-based segmentation methods,[17,18] which were designed based on the elastic (nonrigid) registration of the atlas image to the given image. Nevertheless, these segmentation methods based on direct image registration are unsuitable for resolving the aforementioned difficulties when handling hand MR images.

Recently, some studies related to the bone segmentation for joint motion analysis were presented. Ryu *et al.*[8] utilized a semiautomatic approach to segment hand bones from MR volumetric images of sequentially moving postures. In their method, the thresholds of intensity for distinguishing the bones from their adjacent soft tissues were manually adjusted repeatedly for different bone segments or different image slices while simultaneously removing nonrelevant objects in a laborious process due to the lack of ideal solutions to DY1-DY3. Since the movement of a bone segment between two different postures can be described by using a rigid transformation, a registration-based segmentation scheme is supposed to be ideal for hand moving postural images. Kamojima *et al.*[19] utilized a registration-based method to segment hand bones from images of sequentially moving postures based on many presegmented bone segment models. Liu *et al.*[20] presented a rigid model-based segmentation method for the bones of joints, using an image sequence of joints under different loads. Both strategies intended to fit a segmented bone model into the best matched bone region of the target images by using rigid image registration. Unfortunately, the fitness measures in their registration strategies were not designed for accommodating image artifacts (e.g., DY1-DY2), so their methods might fail to handle the artifact regions of hand MR images. In addition, the articulated model was not utilized, thus the initial posture of each bone model had to be adjusted manually in a tedious and time-consuming endeavor. Up to present, an automatic registration-based segmentation method for whole hand bones is not yet available.

Later, Martín-Fernández *et al.*[21] proposed using an articulated model in the registration of hand radiographies while du Bois d'Aische *et al.*[22] presented a similar registration method for neck MR images. The articulated model utilized a hierarchical relationship wherein the geometric transformations of bones can propagate from high to low layers. With far less movement in the processed images, their models did not provide the joint mechanism that constrains the motion of bone segments. Hence, the transformation correlating the hand moving postural images is still unavailable. (i.e., DY4 has not yet been overcome).

In this paper, we propose a new registration-based method consisting of model-based registration and surface refinement steps for segmenting hand bones from multipostural MR images. For each subject, given a reference postural image to construct a reference model, the hand bones in all the other postural images can be automatically segmented. This method involves four obvious improvements over conventional segmentation methods. First, the reference model with joint mechanism is drivable, and thus can be used to generate a set of hand postures that approximate the hand postures of the given subject. Second, the proposed method can achieve automatic initialization of model-based registration in dealing with the images containing major hand movements. Third, the proposed model-based registration method can cope with the aforementioned difficulties of segmentation (DY1-DY3) by using information of bone intensity and constraints of reference model geometry. Finally, we present a surface refinement approach to successfully improve the bone surfaces on the given image with the registered model. The experiments have demonstrated promising results. This paper is organized as follows. Section II shows the details of the proposed method, Sec. III provides the experiments and the discussion, and Sec. IV states the conclusion.

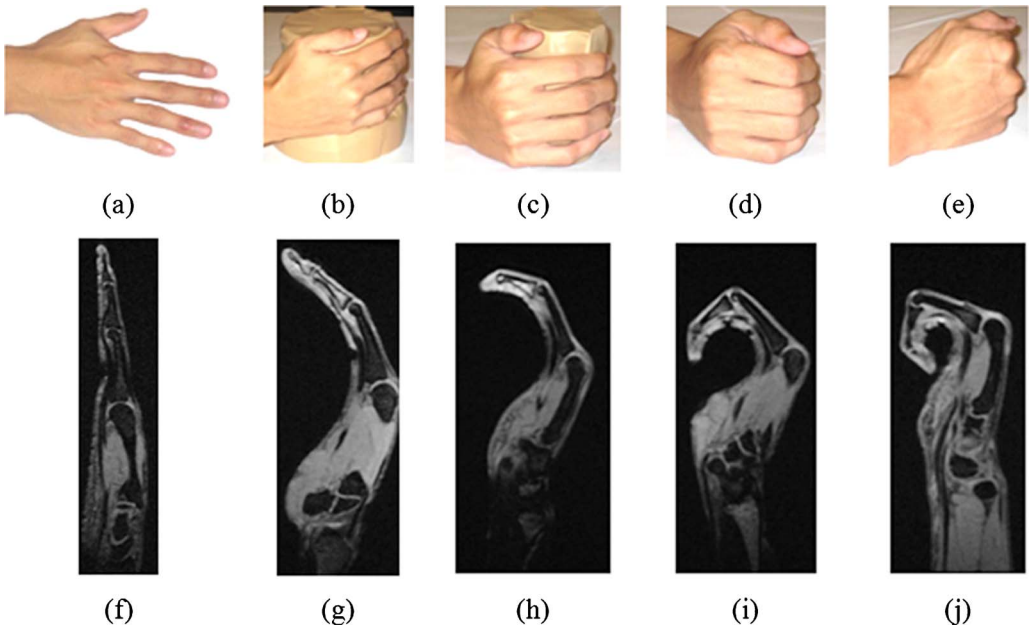

FIG. 2. Five postures of grasping. (a) Neutral posture (posture 1); (b)–(d) intermediate postures between neutral and cage postures; (e) cage posture (posture 5); (f)–(j) sagittal cross-sections selected from the MR volumetric images of postures 1 to 5, respectively.

II. METHOD

II.A. Image preparation

The act of grasping is a popular gesture requiring substantial hand movements and is used as the example to acquire the multipostural images used in this study. While grasping, a hand moves from a neutral posture [Fig. 2(a)] to a cage posture [Fig. 2(e)]; we sampled the motion at five sequential time intervals. The five postures are named as postures 1–5, respectively. The subject grasped different cylinders of various diameters in order to fit the five postures for image acquisition. The hand MR volumetric images were acquired with a GE Signa Excite system and example frames are shown in Figs. 2(f)–2(j), respectively. The imaging protocol that we adopted was a 3D gradient echo sequence with fat suppression by a repetition time of 36 ms (ms), an echo time of 4 ms, and a flip angle of 10°. The pixel size was 0.86×0.86 mm^2.

II.B. Overview of the proposed method

The proposed method starts with the model construction stage, and then applies the constructed model to the registration-based segmentation stage to segment the hand bones from the multipostural images. The flowchart of the proposed method is illustrated in Fig. 3. First, with some manual adjustments, we semiautomatically construct a reference model based on the neutral postural image, including the shape and intensity information of hand bones, and the finger joint mechanism. The reference model is then drivable after initializing the joint parameters (JPs) which are used to simulate the finger joint mechanism.

In the registration-based segmentation stage, the reference model is first registered to the corresponding hand bone regions in a given postural image by using the model-based registration. Then, the surface refinement step based on a deformable model-based framework is utilized to refine the superimposition between the registered reference model and target bone boundaries. To obtain the JPs which better match the joints of the given subject, we further propose a joint parameter refinement process to refine the JPs. Consequently, we can successfully segment the hand bones from the multipostural images based on the drivable reference model. Hand bone motion animations which are helpful for clinicians to understand hand bone geometries in dynamic postures can then be generated based on the segmented postures. The details of the proposed method are described in the following sections.

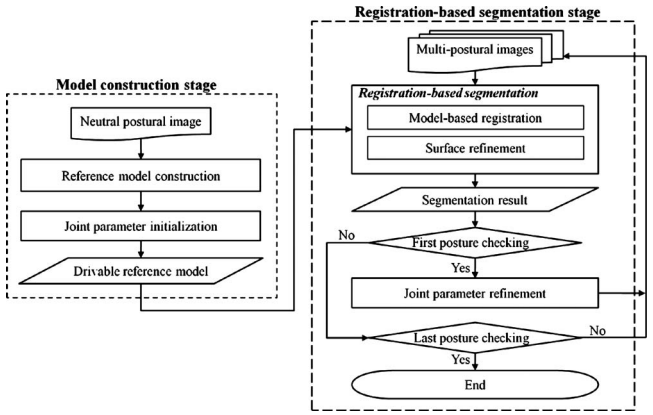

FIG. 3. Flowchart of the proposed method.

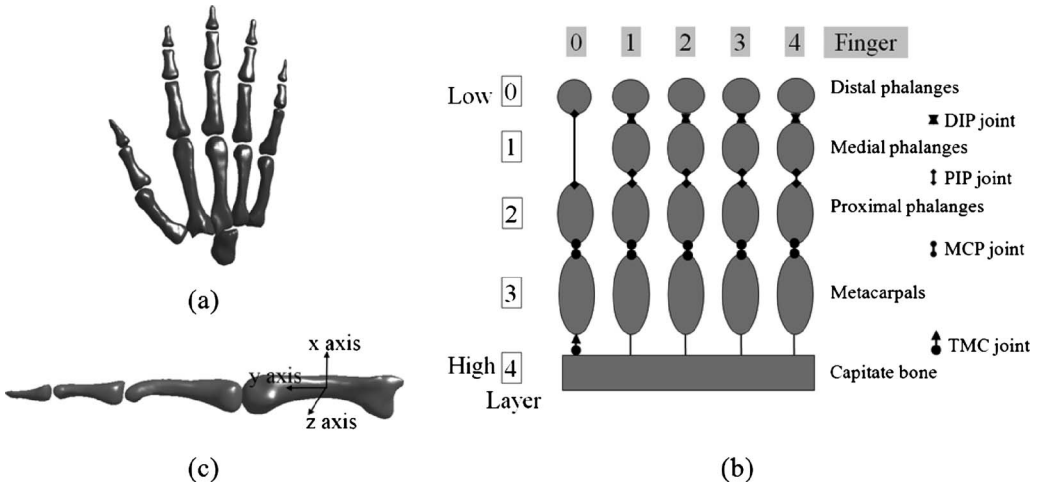

FIG. 4. Architecture of the reference model: (a) Surfaces of the bone components; (b) hierarchical chain relationship of the reference model; (c) bone coordinate system. The arrangements of the bone segments in (a) and (b) are the same.

II.C. Reference model construction

II.C.1. Architecture of the reference model

The reference model used to control the articulated motion of the finger bone segments plays a pivotal role in the proposed registration-based segmentation. The model consists of 20 pieces of bone components, including the capitate bone of the wrist, five metacarpals, five proximal phalanges, four medial phalanges, and five distal phalanges. These bone components are semiautomatically extracted from the neutral postural image using the livewire approach.[20] The bone surfaces of the reference model are triangulated using the marching cube algorithm[23] and then smoothed to remove local fluctuations, as shown in Fig. 4(a).

The human hand is an articulated object so it can be modeled as a hierarchical chain composed of several linked bone segments as shown in Fig. 4(b). In this figure, gray nodes represent the bone segments and their anatomical names are noted on the right. Fingers 0–4 represent the thumb, index, middle, ring, and little fingers, respectively. To provide the characteristics of hand motion, a hierarchy is established with layers descending from the capitate bone to the distal phalanges. The capitate bone is the highest layer that determines global hand motion while the lower layers represent movements of finger bone segments. The geometric transformations of bone segments propagate from the high to low layers in the hierarchy. The hierarchical relationship of hand bones is consequently characterized in the reference model.

II.C.2. Finger joint mechanism of the reference model

Generally, finger motion depends on the integrated movement of the finger bone segments constrained by the finger joint mechanism. Each finger joint has a certain DoF that constrains the rotation of a finger bone segment with respect to its proximally adjacent bone. In fingers 1–4, the metacarpophalangeal (MCP) joint [see Fig. 4(b)] is characterized with two DoFs corresponding to the flexion/extension and adduction/abduction motions. The proximal interphalangeal (PIP) joint and distal interphalangeal (DIP) joint are simple hinge joints with only one DoF corresponding to the flexion/extension motion. On the other hand, the thumb (finger 0), which contains the PIP, MCP, and trapeziometacarpal (TMC) joints, is very different from the other fingers anatomically.[24,25] The first is a hinge joint with one DoF, and the two others are modeled with two-DoF joints, respectively.[26] Consequently, 21 DoFs are assigned to the joints of the reference model totally.

II.C.3. Intensity pattern of the reference model

In addition to the finger joint mechanism, the proposed reference model is also characterized by intensity information of the MR image. Among the multipostural MR images, the intensity distribution of both the bone and its vicinity in a postural image is related to one of the corresponding regions in the other postural images. In order to provide the model with MR intensity information, for each reference bone segment, we build an intensity pattern of the bone and its vicinity from the neutral postural image. The first step requires constructing an oriented bounding box with faces that are parallel to the coordinate planes of the reference bone segment. The intensity pattern is defined as the intensity sequence of the bone bounding box, denoted as a one-dimensional vector $\mathbf{A}_{r,j}=(I_1(\mathbf{BB}_{r,j}(1)),I_1(\mathbf{BB}_{r,j}(2)),\ldots,I_1(\mathbf{BB}_{r,j}(N_1-1)),\times I_1(\mathbf{BB}_{r,j}(N_1)))$, where $\mathbf{BB}_{r,j}$ represents the 3D coordinates of voxels inside the bone bounding box, N_1 is the number of voxels, and I_1 is the neutral postural image. The reference model thus contains the intensity information through reference to a set of intensity patterns of bone segments.

II.D. Joint parameter initialization

In the proposed method, we use the JPs to simulate the joint mechanism of the reference model. In DIP and PIP joints, the JPs consist of a rotation center and a rotation axis;

in MCP and TMC joints, the JPs include a rotation center and two orthogonal rotation axes that intersect at the center. To estimate the JPs of the given subject, at least two known postures are required for analyzing its joint motions. At this stage, only the neutral posture is available; thus for each joint we initially locate the rotation center at the distal head of the corresponding proximally adjacent bone, and assign the rotation axes by following the bone coordinate systems according to the recommendations[27] of the International Society of Biomechanics (ISB). An example illustrating the metacarpal coordinate system of the middle finger is shown in Fig. 4(c). The y-axis is the direction from the mass of center (CoM) of the bone segment to the center of its distal head, and is also regarded as the longitudinal axis of the bone. The x-axis is determined from an x-y sagittal plane splitting the bone segment into mirror images. The z-axis is determined by the right hand rule on the x and y axes.

Based on the bone coordinate systems, we can initialize the rotation axes in the finger joints. The rotation axis in a DIP joint is parallel to the z-axis of the medial phalange, which is the proximally adjacent bone of the DIP joint. Then, the rotation axis in a PIP joint is determined similarly. For MCP joints, the first of the two rotation axes is parallel to the z-axis of its proximally adjacent bone, and the second is perpendicular to both the first rotation axis and the y-axis of the proximal phalange, which is the distally adjacent bone. In the TMC joint of the thumb, the two rotation axes are simply defined as the x and z axes of the metacarpal, respectively.

After the joint parameter initialization, the joint motion can be approximated using a geometric transformation $\mathbf{M}_{r,j}$, where r and j represent the layer value and the finger number of the corresponding bone segment, respectively. $\mathbf{M}_{r,j}$ can be expressed as a product of rotation matrices; each rotation matrix corresponds to a DoF of the corresponding joint motion, and is formed by a rotation axis of the JPs and a given rotation angle. By applying $\mathbf{M}_{r,j}$ to the corresponding reference bone segment, the segment can be rotated with respect to its proximally adjacent bone, driving the reference model to a specific posture.

II.E. Registration-based segmentation

II.E.1. Model-based registration

In the proposed model-based registration, a hierarchical framework is designed to register the reference bone segments to the corresponding bone regions of the given postural image I_k. For each bone segment, the registration process requires three steps which are initial position determination, intensity pattern matching, and intensity optimization. The registration of each bone segment propagates from high to low layers in the hierarchy of model. In each layer, the bone segments are processed from finger 0 to finger 4. After all the bone segments are registered, the hand postures of the given image I_k can be readily identified.

II.E.1.a. Initial position determination. Real hand fingers can support different hand postures with their many DoFs. Without situating the reference bone segment in a proper initial position in the given postural image I_k, the registration method may be constrained in an incorrect local solution. In the proposed system, we present an efficient approach for placing the reference bone segments in the proper positions in I_k, thereby facilitating the subsequent registration.

Usually, capitate bone positions in different postural MR images are not fixed. The capitate bone of the reference model is manually placed in an initial position and then registered using the intensity pattern matching and intensity optimization steps. Since the metacarpal movements relative to the capitate bone are very limited in fingers 1 to 4, their initial positions can be determined by propagating the geometric transformation of the capitate bone to these metacarpals. Furthermore, the hand bone segment is supposed to be located inside the hand region regardless of the postures, so we can determine the initial position of each finger bone segment based on this property.

Articulated object surface, silhouette, or region information is frequently used to help estimate an object posture.[28,29] In the proposed method, an anisotropic smoothing filter is first used to remove image noises, followed by thresholding, morphological dilation, and then hole-filling of the filtered image. The hand region can be extracted and then represented by using a binary image H_k. In the processing window, $H_k(x)$ is assigned with 1 in the hand region and is 0 otherwise, where x is the coordinate of a voxel. Then, the initial position of the bone segment can be determined by maximizing the overlapped region of the reference bone segment and low intensity voxels of I_k inside the processing window

$$\hat{\Theta}_{r,j} = \arg\max_{\Theta_{r,j}} \sum_{i=1}^{N_2} [H_k(\mathbf{M}_{r,j}\mathbf{B}_{r,j}(i))(255 - I_k(\mathbf{M}_{r,j}\mathbf{B}_{r,j}(i)))], \quad (1)$$

where $\Theta_{r,j}$ represents the rotation angle set of the corresponding joint motion, and each element of the set is a rotation angle corresponding to a DoF of the joint motion. $\mathbf{B}_{r,j}$ represents the 3D coordinates of voxels inside the reference bone segment and N_2 denotes the number of voxels. Since hand anatomy restricts finger motion, the rotation angle of a finger bone segment is supposed to be in a certain interval[30] and the finger cannot overly hyperextend. Thus, the maximization process of Eq. (1) is subject to these constraints, so that the estimated rotation angle set $\hat{\Theta}_{r,j}$ can satisfy the motion configuration of a normal hand. By using the joint mechanism with the estimated rotation angle set, the reference bone segment can be driven to the initial position as the first registration step.

II.E.1.b. Intensity pattern matching. After determining the initial position of the reference bone segment, we present an intensity pattern matching algorithm to register the reference bone segment to the corresponding region in the given postural image I_k. We solve registration parameters denoted as $\mathbf{T}_{r,j}$ by maximizing a fitness function that represents the similarity of intensity patterns between the model and the given image. The registration parameters include a transla-

tion vector $\mathbf{t}$ and a rotation matrix $\mathbf{R}$ with respect to the coordinate of reference bone segment. The fitness function is defined as

$$f_{\text{intensity\_pattern}}(\mathbf{T}_{r,j}) = \frac{\text{corr}(\mathbf{A}_{r,j}, \mathbf{A}'_{r,j})}{C_{\text{geometry}}}, \tag{2}$$

where $\mathbf{A}_{r,j}$ is the intensity pattern inside the bone bounding box of the reference bone segment described in Sec. II C 3, and $\mathbf{A}'_{r,j} = (I_k(\mathbf{T}_{r,j}(\mathbf{BB}_{r,j}(1))), I_k(\mathbf{T}_{r,j}(\mathbf{BB}_{r,j}(2))), \ldots, I_k(\mathbf{T}_{r,j}(\mathbf{BB}_{r,j}(N_1-1))), I_k(\mathbf{T}_{r,j}(\mathbf{BB}_{r,j}(N_1))))$ represents the intensity sequence of I_k inside the bone bounding box after $\mathbf{T}_{r,j}$ transformation. By maximizing the correlation coefficient of $\mathbf{A}_{r,j}$ and $\mathbf{A}'_{r,j}$, we can obtain the registration parameters that map the reference bone segment to a region of I_k with the most analogous intensity distribution to the reference intensity pattern. C_{geometry} is used to maintain the geometric structure of the reference model in the matching process. The geometry constraint is defined as

$$C_{\text{geometry}} = C_h + C_b, \tag{3}$$

where C_h is hand surface constraint and C_b is bone position constraint. C_h is formulated as

$$C_h = \sum_{i=1}^{N_2} (255 - H_k(\mathbf{T}_{r,j}(\mathbf{B}_{r,j}(i)))), \tag{4}$$

where H_k represents the extracted hand region. When the reference model exceeds the hand region, C_h will increase and the fitness function of $\mathbf{T}_{r,j}$ will be penalized and become lower, thus avoiding incorrect matching.

In addition, mismatching may occur in the bone segments of fingers 1–4 due to their similarity in both shape and intensity pattern. The bone segments of finger 0 and the capitate bone are less problematic because their shapes and intensity patterns are dissimilar to those of the other bone segments. Therefore, bone position constraint C_b is only designed for the bone segments of fingers 1–4 to maintain the normal articulated structure of the reference model.

Whereas the metacarpals of fingers 1–4 that constitute the palm have very limited motions relative to each other, the phalanges have different joint structures and are more articulate. Therefore, we design the bone position constraints for the metacarpals and phalanges differently. For metacarpals, C_b is defined as

$$\mathbf{C}_b = \begin{cases} 1, & \text{if} \|\mathbf{C}'_j - \mathbf{C}_j\| \le 0.2 * \|\mathbf{C}_j\| \\ \exp\left(\dfrac{\|\mathbf{C}'_j - \mathbf{C}_j\|}{0.2^* \|\mathbf{C}_j\|} - 1\right), & \text{if} \|\mathbf{C}'_j - \mathbf{C}_j\| > 0.2 * \|\mathbf{C}_j\| \end{cases}, \tag{5}$$

where $\mathbf{C}_j$ and $\mathbf{C}'_j$ are the distance vectors from the CoMs of $\mathbf{B}_{r,j}$ and $\mathbf{T}_{r,j}(\mathbf{B}_{r,j})$ to the CoM of the metacarpal in finger $j-1$, respectively. $\mathbf{C}_j$ is calculated from the reference model in the neutral posture. If the difference between $\mathbf{C}_j$ and $\mathbf{C}'_j$ is greater than a given threshold, the estimated palm structure is assumed distorted. The fitness function of $\mathbf{T}_{r,j}$ is thus penalized by a larger C_b, and its value will be decreased.

For phalanges, the bone position constraint is designed as

$$C_b = |\mathbf{T}_{r,j}(\mathbf{B}_{r,j}) \cap \mathbf{B}_{r+1,j}| + |\mathbf{T}_{r,j}(\mathbf{B}_{r,j}) \cap \mathbf{B}_{r,j-1}| + \begin{cases} a, & \text{if } D_1 \le D_2 \\ \kappa^*(D_1 - D_2), & \text{if } D_1 > D_2 \end{cases}, \tag{6}$$

where D_1 denotes the closest distance between the points in the bone segment of layer r and the points in the bone segment of layer $r+1$ (proximally adjacent bone) in finger j of the registered reference bone model, and D_2 is the closest distance between the points in the bone segment of layer r and the points in the bone segments of layer $r+1$ of the neighboring fingers. a is assigned with 1 to avoid the zero-dividing problem and κ is a large positive constant that is currently set as 100 000 in our experiments. In Eq. (6), the first two terms represent improper overlap with the neighboring bone segments, where $\mathbf{B}_{r+1,j}$ is the neighboring bone segment of the same finger and $\mathbf{B}_{r,j-1}$ is the same bone segment of the neighboring finger. The last term prevents the mismatching between the registered bone segment and the other fingers. If D_1 is larger than D_2, this constitutes a mismatching and the fitness function of $\mathbf{T}_{r,j}$ will be penalized by a larger C_b.

II.E.1.c. Intensity optimization. After the intensity pattern matching, the reference bone segment can be closely allocated to the corresponding bone region in the given image I_k. Nevertheless, due to soft tissue deformation or differences in imaging conditions, intensity pattern matching may not necessarily achieve perfect alignment. Therefore, we present an intensity optimization step that minimizes the sum of bone intensity in the *T*2-weighted fat-suppressed images, in which the bone regions are supposed to be dark. If the reference bone segment is exactly registered to the corresponding bone region of I_k, the sum of intensity inside the bone segment should be minimized. The intensity optimization step is achieved by maximizing

$$f_{\text{intensity}}(\mathbf{T}_{r,j}) = \frac{\sum_{i=1}^{N_2} (255 - I_k(\mathbf{T}_{r,j}(\mathbf{B}_{r,j}(i))))}{C_{\text{geometry}}}. \tag{7}$$

The maximization of $f_{\text{intensity}}$ can find a rigid transformation that maps the reference bone segment to the region with the minimal sum of intensity inside I_k. Consequently, we can register the reference bone segment to the corresponding bone region in I_k more precisely.

II.E.2. Surface refinement

Due to inconsistent imaging and physiological conditions, the registered image usually varies with respect to the acquired images of different postures. In addition, the surface-smoothing step in the model construction stage may also cause deviations between the bone boundaries of the reference model and the given postural MR images. Since the previous rigid registration step only adjusts the model posture, it cannot resolve these bone boundary deviations. Thus we propose a snake-based approach to refine the surfaces of bone segments.

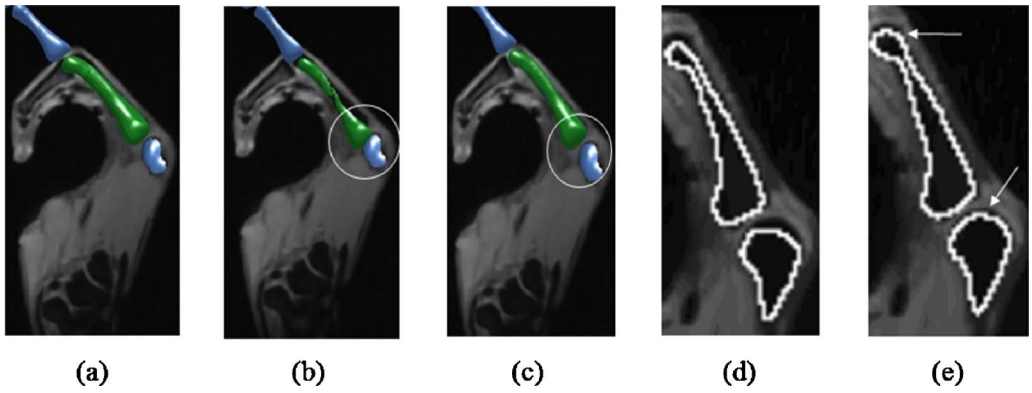

FIG. 5. Intermediate step results in the proposed registration-based segmentation: (a) Initial position of the reference bone segment; (b) registration result without using C_{geometry}; (c) registration result with C_{geometry}; (d) overlaid contours between the registered bone surfaces and cross-sectional image before surface refinement; (e) overlaid contours after surface refinement.

The surface of each bone segment of the registered reference model is refined via minimizing energy E_{refine}

$$E_{\text{refine}}(\tilde{\mathbf{v}}_i) = \sum_{i=0}^{N_3} [\alpha E_{\text{shape}}(\tilde{\mathbf{v}}_i) + (1-\alpha)(E_{\text{edge}}(\tilde{\mathbf{v}}_i) + E_{\text{region}}(\tilde{\mathbf{v}}_i))], \tag{8}$$

where E_{shape} represents the shape energy, E_{edge} is the edge energy, E_{region} is the region energy, α is a weighting value, $\tilde{\mathbf{v}}_i$ represents the coordinate of the ith vertex, and N_3 is the number of vertices on the deformable model. The shape energy that restricts the movement of vertex on the deformable model is defined as

$$E_{\text{shape}}(\tilde{\mathbf{v}}_i) = \sum_{j \in \text{Nei}(i)} \left| \left(\frac{\mathbf{v}_j - \mathbf{v}_i}{\|\mathbf{v}_j - \mathbf{v}_i\|} \right) \cdot \left(\frac{\tilde{\mathbf{v}}_j - \tilde{\mathbf{v}}_i}{\|\tilde{\mathbf{v}}_j - \tilde{\mathbf{v}}_i\|} \right) - 1 \right|, \tag{9}$$

where $\mathbf{v}_i$ is the coordinate of the ith vertex on the original model before deformation, and $\text{Nei}(i)$ represents its neighboring vertices. By referring to the local shape features of the original model, E_{shape} closely maintains the shape of the deformable model to the original in the deformation process, to help avoid excessive distortions.

The edge and region energies that measure the boundary fitness between the deformable model and the underlying image are designed as follows:

$$E_{\text{edge}}(\tilde{\mathbf{v}}_i) = I_k(\tilde{\mathbf{v}}_i) - I_k(\tilde{\mathbf{v}}_i + \mathbf{n}(\tilde{\mathbf{v}}_i)), \tag{10}$$

$$E_{\text{region}}(\tilde{\mathbf{v}}_i) = \sum_{a=-L}^{-1} |I_k(\tilde{\mathbf{v}}_i + a\mathbf{n}(\tilde{\mathbf{v}}_i)) - c_1|^2 + \sum_{a=1}^{L} |I_k(\tilde{\mathbf{v}}_i + a\mathbf{n}(\tilde{\mathbf{v}}_i)) - c_2|^2, \tag{11}$$

where $\mathbf{n}(\tilde{\mathbf{v}}_i)$ denotes the outward normal vector, $\tilde{\mathbf{v}}_i + a\mathbf{n}(\tilde{\mathbf{v}}_i)$ represents a voxel on the search line, L is the half length of the search line, and c_1 and c_2 represent the average intensity values along the search line inside and outside the model surface. The bone boundaries in fat-suppressed $T2$-weighted MR images are expected to appear in the transition from low to high intensity, while the intensities near the boundary position are two-clustered with sharp changes. By using the E_{edge} and E_{region}, the deformable model can be attracted to the bone boundaries of the given image.

Equation (8) is optimized by iteratively adjusting the positions of vertices of the deformable model to fit the true bone boundaries along the normal directions of vertices. The iteration converges and stops when the sum of displacements of vertices between the previous and current iterations is less than 1, or if the number of iteration reaches 25. On the other hand, the deformable model behavior can be controlled by adjusting the weighting values α of Eq. (8). In our experiments, they are empirically assigned; the value of α for vertices which belong to the distal and proximal ends is given the value 0.2. For those vertices in the other regions of the deformable model, a larger α value 0.8 is adopted for better resistance to the attraction from the confusing edges of soft tissues, such as tendons. The adopted half length L of the search line is 4.

Figure 5 shows the intermediate results of two steps in the proposed registration-based segmentation. Given an initial position of the reference bone segment [Fig. 5(a)], the segment is registered to its corresponding bone region in the given postural image by using model-based registration. The currently processed bone segment of reference model is represented in green and the other segments are in blue. Figure 5(b) shows the registration result without using the geometry constraint, while Fig. 5(c) presents the one confined with the constraint. Unreasonable registration results, such as the intersection of the reference segment with its proximally adjacent one (circled area), can be resolved after applying the geometry constraint. Figures 5(d) and 5(e) demonstrate the resulting bone contours before and after the surface refinement step. Undesirable shape deviations are removed after the refinement step, as indicated by the arrows.

II.F. Joint parameter refinement

In the proposed registration-based segmentation method, we utilize the JPs to determine the joint motions so that the

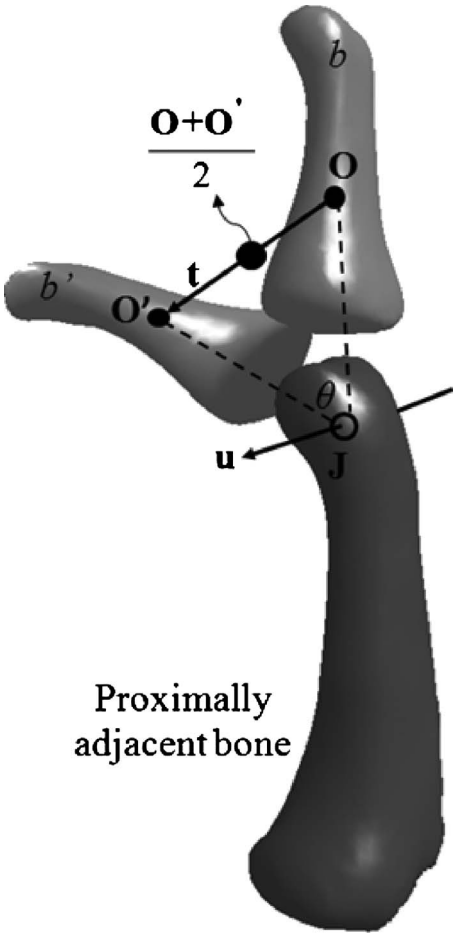

FIG. 6. Illustration for estimating the JPs.

reference model can be driven to a specific hand posture. However, the initial JPs assigned based on the recommendations of the ISB are usually sensitive to bone coordinate deviations. Using improper JPs may not achieve a good posture approximation in the model-based registration and may cause an unstable registration. We thus propose a joint parameter refinement step to resolve this problem.

To obtain the JPs that better match the joints of the given subject, we require at least his/her two known postures. The cage posture, which has the largest joint motion with respect to the neutral posture, is helpful to refine the JPs of the reference model. Thus, the cage postural image is selected as the first posture in the segmentation stage and then its segmentation results are used to refine the initial JPs of the reference model. The geometric transformation $\mathbf{T}_{r,j}$ of a reference bone segment with respect to its proximally adjacent bone between the neutral and cage postures can be obtained from the model-based registration step. $\mathbf{T}_{r,j}$ includes a rotation matrix $\mathbf{R}=[[r_{11}r_{21}r_{31}]^T[r_{12}r_{22}r_{32}]^T[r_{13}r_{23}r_{33}]^T]$ and a translation vector $\mathbf{t}=[t_x t_y t_z]^T$. From the geometric transformation of this movement, we can estimate the JPs of the given subject.

Constrained by the joint DoF, rotational motion can approximate the movement of the finger bone segment. In Fig. 6, bone segment b rotates around axis $\mathbf{u}$ located at point $\mathbf{J}$, with rotation angle θ. The bone segment, after the rotation, is represented by b'. $\mathbf{O}$ and $\mathbf{O}'$ represent the CoM of b and b', respectively. Given the rotation matrix $\mathbf{R}$, rotation axis $\mathbf{u}$ and rotation angle θ are retrieved based on Euler's rotation theorem[31]

$$\mathbf{u}=\frac{1}{2\sin\theta}\begin{bmatrix} r_{32}-r_{23} \\ r_{13}-r_{31} \\ r_{21}-r_{12} \end{bmatrix},$$

$$\theta=\arccos\left(\frac{r_{11}+r_{22}+r_{33}-1}{2}\right). \tag{12}$$

In Fig. 6, triangle $\mathbf{JOO}'$ is isosceles, based on the assumption that the movement between b and b' is a single planar rotational motion. Therefore, the rotation center $\mathbf{J}$ can be calculated by

$$\mathbf{J}=\frac{\mathbf{O}+\mathbf{O}'}{2}+\frac{\mathbf{u}\times\mathbf{t}}{\|\mathbf{u}\times\mathbf{t}\|}\left(\frac{\frac{\|\mathbf{t}\|}{2}}{\tan\left(\frac{\theta}{2}\right)}\right),$$

$$\mathbf{t}=\mathbf{O}'-\mathbf{O}. \tag{13}$$

Using Eqs. (12) and (13), we can estimate the JPs which are the rotation axes and rotation center for the movement of a finger bone segment.

The DIP and PIP joint motions with one DoF which corresponds to the flexion/extension are constrained with one rotation axis by using Eqs. (12) and (13). On the other hand, the MCP and TMC joints with two DoFs are constrained by two rotation axes. Thus, the bone posture can be obtained by adjusting the rotation angles, such that the simulated joint mechanism in the two-DoF joints is less influenced by the deviations of bone coordinates. Adopting the definitions of rotation axes recommended by the ISB can well approximate the hand postures of a given subject, so we need only estimate the rotation center and adopt the ISB-defined rotation axes for the two-DoF joints. As the JPs are directly estimated based on the image data, the resulting JPs are less sensitive to bone coordinate deviations and can better match the joint motion behaviors of the given subject. For each subject, the JPs are automatically determined based on two postural images at the beginning of the registration step. Since the joint model of each subject physically varies very little during finger motion, the JPs can be used to match all other images for the same subject once they are determined. In other words, the subject-specific reference model can be used in registering different postural images or even images from different acquisition of the same subject.

II.G. Hand bone motion animation

To provide the clinicians with the dynamic information of hand bone geometries, we generate the hand bone motion animations by interpolating frames between sequentially moving postures segmented from the MR images. The inter-

polation between the source and target postures is achieved by using the proposed finger joint mechanism

$$\mathbf{V}_{r,j}^{t}=\left(\prod_{a=0}^{4-r}\mathbf{M}_{4-a,j}^{t}\right)\mathbf{V}_{r,j}^{0}, \tag{14}$$

where $t\in[0,1]$ is the time index in the whole motion sequence. The source and target postures are specified with t equals to 0 and 1, respectively. $\mathbf{V}_{r,j}^{t}$ represents the surface of the bone segment of layer r in finger j in the frame at time t and $\mathbf{V}_{r,j}^{0}$ is the surface of the corresponding bone in the source posture. $\mathbf{M}_{4-a,j}^{t}$ represents a 3D geometric transformation that indicates the corresponding joint motion between the source and target postures in the frame at time t. By using Eq. (14), we can automatically generate proper postures in the interpolating trajectory and conveniently obtain smooth and realistic animations of hand motion.

III. EXPERIMENTS AND DISCUSSION

The following experiments consist of three parts: (1) Visual evaluation, (2) quantitative analysis, and (3) comparison with three other segmentation methods. In the following experiments, the multipostural image data from four subjects were included in the validation work. For each subject, the neutral, cage, and at least one intermediate postures were selected in the acquisition of his/her multipostural images. The neutral postural image was utilized to construct the reference model, and the others were used to test the proposed segmentation method. The hand bones in the test images were automatically segmented based on the constructed model. The system parameters including the distance ratio in Eq. (5) and the weights of the deformable model in Eq. (8) were determined based on the image data of subject 1. As these parameters are the relative measures (e.g., ratio) of energy or geometry features, they are less sensitive to the shape variation and intensity distribution of different hands. The same parameters were used throughout the experiments on all subjects.

III.A. Visual evaluation

The segmentation results of hand bones from the postural images of subject 1 are shown in Fig. 7. The top row demonstrates surfaces of the resulting bones, which mimic the true anatomical appearance of bone segment with realistic shapes and smooth surfaces. The center and bottom rows of Fig. 7 demonstrate the resulting bone contours by superimposing the surfaces onto coronal, sagittal and axial cross-sectional MR images. Overall, the segmented contours highly agree with the true bone boundaries in the validation data, even in the presence of the aforementioned segmentation difficulties indicated by the solid, open-headed, and dashed arrows (DY1, DY2, and DY3, respectively). In addition, based on the segmented postures, we also generated the hand bone motion animations by using Eq. (14). The animations are helpful for the clinicians to understand and assess the dynamic changes in hand bone geometries. More segmentation results of the other subjects and demonstrations of the hand motion animations are available on our web page.[32]

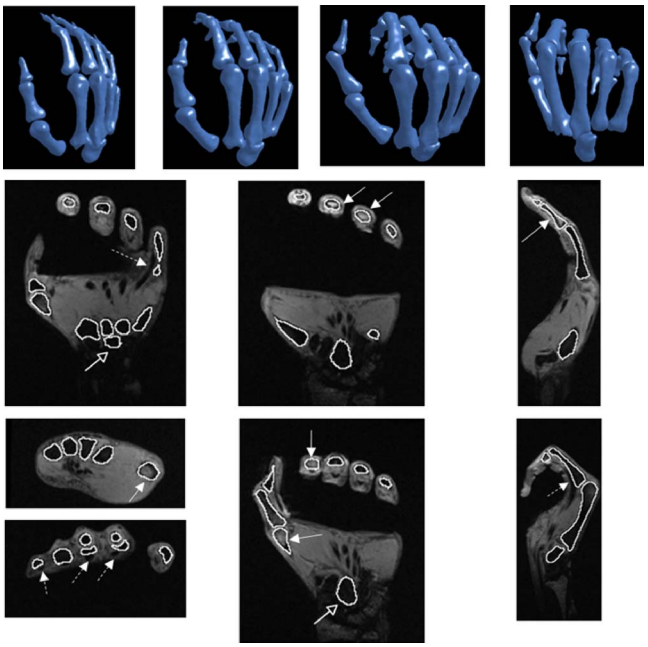

FIG. 7. Segmentation results of hand bones from the validation postural images using the proposed method. The top row shows the surfaces of segmented bones. The center and bottom rows demonstrate the overlaid contours between the bone surfaces and cross-sectional images.

III.B. Quantitative analysis of the segmentation results

In the quantitative analysis, the segmentation results by the proposed automatic method were compared against the average of manual results of two experts, which constituted the ground truth for validating the accuracy of the proposed method. Since manual segmentation of the whole data set (ten postural image volumes in this experiment) was tedious and impracticable, we chose the four bone segments (i.e., the distal, medial, and proximal phalanges and metacarpal) of the middle finger from each postural image volume for validation. For each of the four bone segments, the comparison was achieved based on three metrics, including the mean error (ME), the root mean square error (RMSE), and the dice similarity coefficient[33] (DSC)

$$\mathrm{ME}=\sum_{i=1}^{N}\sqrt{(\mathbf{a}_i-\mathbf{b}_j)^2}/N, \tag{15}$$

$$\mathrm{RMSE}=\sqrt{\sum_{i=1}^{N}(\mathbf{a}_i-\mathbf{b}_j)^2/N}, \tag{16}$$

$$\mathrm{DSC}=\frac{2|\mathbf{A}\cap\mathbf{G}|}{|\mathbf{A}|+|\mathbf{G}|}, \tag{17}$$

where $\mathbf{a}_i$ is the ith surface point of the automatic result, $\mathbf{b}_j$ is the jth surface point of the ground truth that is the closest to $\mathbf{a}_i$, and N is the number of surface points of the automatic

TABLE I. Means and standard deviations of accuracy measures (ME, RMSE, and DSC) estimated from the proximal, medial, distal phalanges, and metacarpal of the middle finger in the multipostural images of four subjects.

Subject	Posture	Average ME (mm)	Average RMSE (mm)	Average DSC (%)
1	2	0.668 ± 0.012	0.689 ± 0.011	84.752 ± 7.321
	3	0.634 ± 0.027	0.707 ± 0.051	83.724 ± 6.938
	4	0.601 ± 0.027	0.652 ± 0.038	86.143 ± 3.656
	5	0.666 ± 0.046	0.712 ± 0.028	84.491 ± 6.249
2	3	0.613 ± 0.029	0.656 ± 0.036	84.799 ± 7.071
	5	0.614 ± 0.018	0.651 ± 0.024	85.317 ± 4.426
3	4	0.726 ± 0.044	0.777 ± 0.052	82.815 ± 6.276
	5	0.683 ± 0.077	0.731 ± 0.063	82.760 ± 5.865
4	4	0.560 ± 0.064	0.629 ± 0.066	85.068 ± 4.416
	5	0.500 ± 0.044	0.588 ± 0.063	84.348 ± 6.330

result. **A** and **G** are the sets of voxels classified as the bone segments in the automatic result and the ground truth, respectively. The ME and RMSE represent the surface distance deviations between the automatic result and the ground truth. The DSC is a measure of the spatial dependency between two segmented bone volumes, and its value ranges from zero, indicating no overlap, to one indicating complete overlap.

Table I states the evaluation results and each row of the table lists the average ME, RMSE, and DSC of the four bone segments in the middle finger, respectively. As shown in Table I, the average MEs and RMSEs were less than 1 mm and the average DSCs were far above 0.8, indicating a good overlap between the automatic results and the ground truth.[33] Beyond the assessment of segmentation results of the middle finger, we further validated the proposed method with two sets of orthogonal cross-sections to evaluate the results of different bone segments. The validation images included three coronal and three sagittal view images from each of the four postural images of subject 1, and the ground truth was given by the average of manual results by the same two experts. Tables II and III state the resulting distance errors of bone contours and the overlap ratios of bone regions in the coronal and sagittal cross-sectional images, respectively. As shown in Tables II and III, the average MEs were 0.574 ± 0.079 and 0.617 ± 0.077 mm; the average RMSEs were 0.816 ± 0.092 and 0.862 ± 0.079 mm; and the average DSCs were 0.887 ± 0.02 and 0.875 ± 0.02 in coronal and sagittal views, respectively. The resulting MEs and RMSEs were less than 1 mm, and moreover, all the DSC values were larger than 0.8. Overall, the evaluation results are satisfactory for clinical or biomechanics requirements.

III.C. Comparative study

Image segmentation methods have been developed and are widely used in medical image analysis. Although there have been several literatures[5,6] concerning the bone segmentation for joint motion analysis, they do not present solutions for handling the aforementioned difficulties of MR hand bone segmentation. To make these methods accommodate the hand postural MR images thus require large modification or reformation of their segmentation protocols. Therefore, three popular generic methods, which do not utilize the hand bone knowledge, were selected for comparison to show how the proposed ideas can improve the segmentation results. The three selected methods included a region-based method, which is watershed,[34] and two deformable model-based methods, which are Chan–Vese and snake methods, respectively.[15,13] The comparison was achieved by visually evaluating the segmentation results obtained by the proposed and the other three methods.

TABLE II. Accuracy evaluation results in ME, RMSE and DSC estimated from the coronal images of subject 1.

Image no.	ME (mm)	RMSE (mm)	DSC (%)
Posture 2			
2.1.c	0.589	0.840	87.582
2.2.c	0.450	0.698	92.865
2.3.c	0.496	0.755	91.429
Posture 3			
3.1.c	0.607	0.871	88.387
3.2.c	0.630	0.863	86.539
3.3.c	0.715	1.029	89.773
Posture 4			
4.1.c	0.609	0.834	87.467
4.2.c	0.648	0.877	85.489
4.3.c	0.490	0.703	90.527
Posture 5			
5.1.c	0.506	0.745	89.265
5.2.c	0.618	0.818	84.411
5.3.c	0.525	0.756	90.717
Mean ± SD	0.574 ± 0.079	0.816 ± 0.092	88.704 ± 2.521

TABLE III. Accuracy evaluation results in ME, RMSE and DSC estimated from the sagittal images of subject 1.

Image no.	ME (mm)	RMSE (mm)	DSC (%)
Posture 2			
2.1.s	0.524	0.798	90.234
2.2.s	0.592	0.833	88.674
2.3.s	0.601	0.886	89.031
Posture 3			
3.1.s	0.676	0.918	86.911
3.2.s	0.742	0.997	84.906
3.3.s	0.621	0.891	85.974
Posture 4			
4.1.s	0.712	0.892	84.591
4.2.s	0.573	0.800	88.242
4.3.s	0.524	0.751	88.899
Posture 5			
5.1.s	0.713	0.968	85.977
5.2.s	0.531	0.752	90.908
5.3.s	0.591	0.833	86.487
Mean ± SD	0.617 ± 0.077	0.862 ± 0.079	87.569 ± 2.055

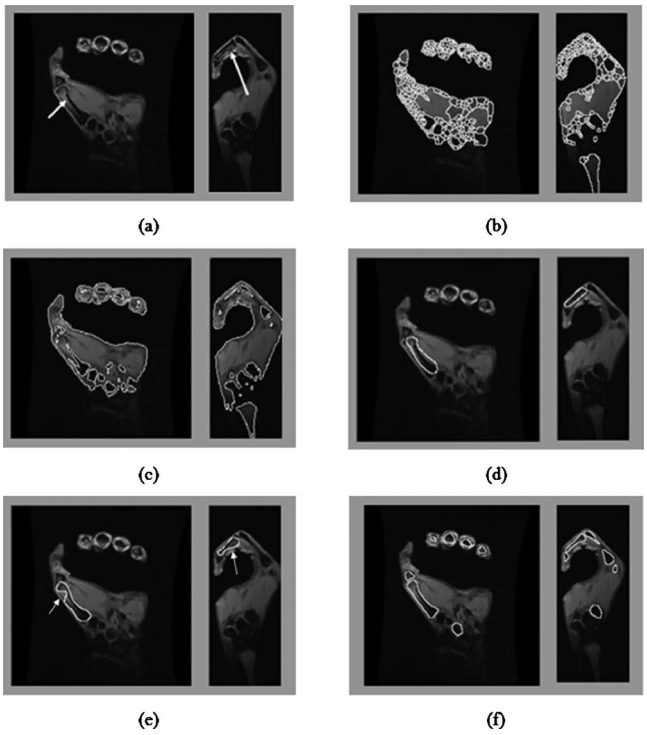

FIG. 8. Comparison study: (a) The original image; (b) the results by watershed method; (c) the results by Chan–Vese method; (d) snake initialization; (e) the results by snake; (f) the results by the proposed method.

Figure 8(a) shows two examples, wherein two conspicuous image artifacts, DY1 and DY3, are indicated by arrows, respectively. As the watershed and Chan–Vese methods segment regions only based on homogeneity of image intensity, it is quite difficult for them to differentiate tissues, such as bones and tendons which are with similar intensity. They thus yielded incorrect tissue regions and many fragmentary contours as shown in Figs. 8(b) and 8(c). The parameters used in the two methods were empirically adjusted to obtain the best results. Moreover, as the conventional snake deformation is only constrained by the bending degree of the deforming surface, it is easily influenced by some undesirable strong edges or image noise. Even though the snake was given an initial model [see Fig. 8(d)] very close to the true bone boundary, incorrect convergence of deformation [see Fig. 8(e)] still resulted due to DY1 and DY3. Finally, Fig. 8(f) shows the results by the proposed method. Compared to the results by the other three methods, our results were more desirable due to the more realistic bone shape and the good fit with bone boundaries in the images. The conventional methods mentioned above do not utilize any bone model information. In contrast, the proposed method acquires the bone shape information from the registered reference model, and thus can successfully handle the difficulties of segmentation in hand MR images and achieve good segmentation results.

IV. CONCLUSION

Hand bone segmentation from MR images is an essential requirement for investigating hand kinematics and pathology. We proposed a new registration-based segmentation method consisting of the model-based registration and surface refinement processes to segment hand bones from multipostural MR images. First, we built a drivable reference model by incorporating the articulated bone structure with a finger joint mechanism. Based on the motion constraints of the joint mechanism, the model region was automatically aligned to the hand region of the given postural image. The intensity pattern matching and intensity optimization steps overcame the difficulties of nonuniform intensity and fuzzy boundaries to obtain the model posture that is best matched to the target image. Finally, we employed a surface refinement step utilizing image gradient, region uniformity, and model shape information to improve the fitness between the registered model and the corresponding bones.

In the experimental results, the proposed automatic method yielded accurate segmentation results with less than 1 mm in ME and RMSE and larger than 0.8 in DSC. It also demonstrated better segmentation results than conventional methods. Thus, the proposed method is helpful to understand hand bone geometries in dynamic postures. In the future, we will try to extend the current method to incorporate hand atlas knowledge for handling intersubject data. Applications for articulated structures (e.g., hand, knee, neck, and spine) will be investigated to quantify the bone motion information before and after treatment for evaluating curative effects.

ACKNOWLEDGMENTS

The authors would like to express their appreciation for the grant under contract NSC 97-2221-E-006-158-MY2 from the National Science Council, Taiwan, Republic of China. This work utilized shared facilities supported by the Program of Top 100 Universities Advancement, Ministry of Education, Taiwan, Republic of China.

[a]Electronic mail: wale1212@gmail.com
[b]Electronic mail: jming@mail.ncku.edu.tw
[c]Electronic mail: n044206@mail.hosp.ncku.edu.tw
[d]Electronic mail: fcsu@mail.ncku.edu.tw
[e]Author to whom correspondence should be addressed. Electronic mail: ynsun@mail.ncku.edu.tw; Telephone: +886-6-2757575 ext. 62526; Fax: +886-6-2747076.

[1]A. H. Makkouk, M. E. Oetgen, C. R. Swigart, and S. D. Dodds, "Trigger finger: Etiology, evaluation, and treatment," Current Reviews in Musculoskeletal Medicine **1**(2), 92–96 (2008).
[2]C. W. Chang, S. P. Ho, Y. N. Sun, L. C. Kuo, C. C. Lin, M. S. Ju, F. C. Su, and I. M. Chou, "Multiple view finger tracking using 3-D model and color features for therapeutic evaluations," in Proceedings of the 16th ICMMB, Pittsburgh, PA, 2008.
[3]F. C. Su, L. C. Kuo, H. Y. Chiu, and M. J. Chen-Sea, "Video-computer quantitative evaluation of thumb function using workspace of the thumb," J. Biomech. **36**, 937–942 (2003).
[4]X. Zhang, S. W. Lee, and P. Braido, "Determining finger segmental centers of rotation in flexion-extension based on surface marker measurement," J. Biomech. **36**, 1097–1102 (2003).
[5]Y. Hu, D. R. Haynor, M. Fassbind, E. Rohr, and W. Ledoux, "Image segmentation and registration for the analysis of joint motion from 3-D MRI," Proc. SPIE **6141**, 133–142 (2006).
[6]J. G. Snel, H. W. Venema, T. M. Moojen, M. J. P. F. Ritt, C. A. Grimbergen, and G. J. den Heeten, "Quantitative in vivo analysis of the kinematics of carpal bones from three-dimensional CT images using a deformable surface model and a three-dimensional matching technique," Med. Phys. **27**(9), 2037–2047 (2000).

[7]N. Miyata, M. Kouchi, M. Mochimaru, and T. Kurihara, "Finger joint kinematics from MR images," in Proceedings of the IEEE/RSJ International Conference on Intelligent Robots and Systems (IROS), Japan, August 2005.
[8]J. H. Ryu, N. Miyata, M. Kouchi, M. Mochimaru, and K. H. Lee, "Analysis of skin movements with respect to bone motions using MR images," J. Biomech. **39**, 844–852 (2006).
[9]L. Kalichman, E. Kobyliansky, and G. Livshits, "Characteristics of joint degeneration in hand osteoarthritis," Jt., Bone Spine **73**, 72–76 (2006).
[10]P. Peloschek, G. Langs, M. Weber, J. Sailer, M. Reisegger, H. Lmhof, H. Bischof, and F. Kainberger, "An automatic model-based system for joint space measurements on hand radiographs: Initial experience," Radiology **245**(3), 855–862 (2007).
[11]L. C. Kuo, H. Y. Chiu, C. W. Chang, H. Y. Hsu, and Y. N. Sun, "Functional workspace for precision manipulation between thumb and fingers in normal hands," J. Electromyogr Kinesiol **19**, 829–839 (2009).
[12]R. H. Hashemi, W. G. Bradley, and C. J. Lisanti, *MRI The Basics*, 2nd ed. (Lippincott Williams & Wilkins, Philadelphia, PA, 2004).
[13]M. Kass, A. Witkin, and D. Terzopoulos, "Snake: Active contour models," Int. J. Comput. Vis. **1**(4), 321–331 (1988).
[14]T. F. Cootes, C. J. Taylor, D. H. Cooper, and J. Graham, "Active shape models—Their training and application," Comput. Vis. Image Underst. **61**(1), 38–59 (1995).
[15]T. F. Chan and L. A. Vese, "Active contour without edges," IEEE Trans. Image Process. **10**(2), 266–277 (2001).
[16]V. Zagrodsky, V. Walimbe, C. R. Castro-Pareja, J. X. Qin, J. M. Song, and R. Shekhar, "Registration-assisted segmentation of real-time 3-D echocardiographic data using deformable models," IEEE Trans. Med. Imaging **24**(9), 1089–1099 (2005).
[17]T. Rohlfing, R. Brandt, R. Menzel, and C. R. Maurer, "Evaluation of atlas selection strategies for atlas-based image segmentation with application to confocal microscopy images of bee brains," Neuroimage **21**(4), 1428–1442 (2004).
[18]M. Bach Cuadra, M. De Craene, V. Duay, B. Macq, C. Pollo, and J.-Ph. Thiran, "Dense deformation field estimation for atlas-based segmentation of pathological MR brain images," Comput. Methods Programs Biomed. **84**(2), 66–75 (2006).
[19]S. Kamojima, N. Miyata, and J. Ota, "Identification of position and orientation of hand bones from MR images by bone model registration," in Proceedings of the IEEE/RSJ International Conference on Intelligent Robots and Systems (IROS), 2004, pp. 2021–2027.
[20]J. Liu, J. K. Udupa, and P. K. Saha, "Rigid model-based 3D segmentation of the bones of joints in MR and CT images for motion analysis," Med. Phys. **35**(8), 3637–3649 (2008).
[21]M. Á. Martín-Fernández, E. Muñoz-Moreno, M. Martín-Fernández, and C. Alberola-López, "Articulated registration-elastic registration based on a wire-model," Proc. SPIE **5747**, 182–191 (2005).
[22]A. du Bois d'Aische, M. De Craene, B. Macq, and S. K. Warfield, "An improved articulated registration method for neck images," in Proceedings of the 27th Annual International Conference of IEEE EMBS, 2005, pp. 7668–7671.
[23]W. E. Lorensen and H. E. Cline, "Marching cubes: A high resolution 3-D surface construction algorithm," (ACM) Computer Graphics **21**(4), 163–169 (1987).
[24]W. P. Cooney, M. J. Lucca, E. Y. S. Chao, and R. L. Linscheid, "The kinesiology of the thumb TMC joint," J. Bone Jt. Surg., Am. Vol. **63**, 1371–1381 (1981).
[25]P. Cerveri, E. De Momi, N. Lopomo, G. Baud-Bovy, R. M. L. Barros, and G. Ferrigno, "Finger kinematic modeling and real-time hand motion estimation," Ann. Biomed. Eng. **35**(11), 1989–2002 (2007).
[26]S. Cobos, M. Ferre, and M. A. Sanchéz-Urán, "Simplified hand configuration for object manipulation," Lect. Notes Comput. Sci. **5024**, 730–735 (2008).
[27]G. Wu, F. C. T. van der Helm, H. E. J. Veeger, M. Makhsous, P. Van Roy, C. Anglin, J. Nagels, A. R. Karduna, K. McQuade, X. Wang, F. W. Werner, and B. Buchholz, "ISB recommendation on definitions of joint coordinate systems of various joints for the reporting of human joint motion—Part II: Shoulder, elbow, wrist and hand," J. Biomech. **38**, 981–992 (2005).
[28]N. Shimada, K. Kimura, and Y. Shirai, "Real-time 3-D hand posture estimation based on 2-D appearance retrieval using monocular camera," in Proceedings of the IEEE/ICCV Workshop on Recognition, Analysis, and Tracking of Faces and Gestures in Real-time Systems, Washington, DC, 2001.
[29]J. Cui and Z. Sun, "Model-based visual hand posture tracking for guiding a dexterous robotic hand," Opt. Commun. **235**, 311–318 (2004).
[30]J. Lin, Y. Wu, and T. S. Huang, "Modeling the constraints of human hand motion," in Proceedings of the IEEE Workshop on Human Motion (HUMO), Los Alamitos, CA, 2000, pp. 121–126.
[31]F. S. Hill and S. M. Kelley, *Computer Graphics Using OpenGL*, 3rd ed. (Prentice Hall, Upper Saddle River, NJ, 2007).
[32]http://image.csie.ncku.edu.tw/research/RBShand.htm
[33]K. H. Zou, S. K. Warfield, A. Bharatha, C. M. Tempany, M. R. Kaus, S. J. Haker, W. M. Wells III, F. A. Jolesz, and R. Kikinis, "Statistical validation image segmentation quality based on a spatial overlap index," Acad. Radiol. **11**, 178–189 (2004).
[34]L. Vincent and P. Soille, "Watersheds in digital spaces: An efficient algorithm based on immersion simulations," IEEE Trans. Pattern Anal. Mach. Intell. **13**(6), 583–598 (1991).